Korean J. Chem. Eng., 35(9), 1836-1843 (2018)
DOI: 10.1007/s11814-018-0094-9

pISSN: 0256-1115
eISSN: 1975-7220

Preparation and characterization of hydrophilic polydopamine-coated Fe_3O_4/oxide graphene imprinted nanocomposites for removal of bisphenol A in waters

Suyu Ren*, Jing Tao, Ying Cui*, Jinsuo Gao*, Xiaona Li*, and Feng Tan*,†**

*Key Laboratory of Industrial Ecology and Environmental Engineering (MOE), School of Environmental Science and Technology, Dalian University of Technology, Dalian 116024, China
**Department of Chemistry & Life Science, Anshan Normal College, Anshan 114005, China
(*Received 27 March 2018 • accepted 4 June 2018*)

Abstract−Bisphenol A (BPA), a known endocrine disruptor, is of global concern because it poses serious threats to the ecological environment and human health. In this work, hydrophilic polydopamine-coated Fe_3O_4/oxide graphene (IPDA@MGO) magnetic imprinted nanocomposites were prepared by the self-polymerization of dopamine on the surface of Fe_3O_4/GO in Tris-HCl buffer using BPA as a template for selective adsorption of BPA in water. IPDA@MGO showed specific recognition toward BPA with a high imprinting factor of 3.2 compared with nonimprinted polymer. The capacity of IPDA@MGO toward BPA was 41.2 mg/g and the adsorption reached equilibrium within 30 min. The adsorption agreed well with the Freundlich and pseudo-second order kinetic models. The good adsorption performance was attributed to the abundant binding sites and good dispersibility of IPDA@MGO nanocomposites derived from its excellent hydrophilicity. The nanocomposites could be removed rapidly by an external magnet and regenerated for repeated adsorption of BPA in water. The proposed method has potential applications for efficient removal of BPA in environmental waters.

Keywords: Adsorption, Bisphenol A, Molecular Imprinting, Nanocomposites, Polydopamine

INTRODUCTION

Endocrine-disrupting compounds (EDCs) are of global concern because they pose serious threats to ecological environment and human health [1,2]. Bisphenol A (BPA) is a known estrogen-like endocrine disruptor that can induce abnormal differentiation of reproductive organs by interfering with the action of endogenous gonadal steroid hormones [3]. Recent research shows that low-dose BPA can result in an increasing risk of diabetes mellitus, cardiovascular diseases and liver enzyme [4]. On the other hand, BPA, as an important chemical, has been widely used in the manufacture of polycarbonate plastics and epoxy resins for plastic products such as water bottles, baby bottles, food containers and dental sealants. This results in release of BPA into aquatic environments, posing an exposure risk of BPA to aquatic organisms and human. Many studies have detected BPA in surface water, ground water, and sea water [5-8]. Thus, efficient removal of BPA in water is highly desirable.

Various techniques have been applied to eliminate BPA in water, including advanced oxidation [9], membrane bioreactor [10], microbial degradation [11], photodegradation [12], nanofiltration [13], and adsorption [14,15]. Among these, adsorption has shown many advantages, including less energy consumption, ease of operation, and low cost of maintenance. Common adsorbents for the removal of BPA include clay [16], zeoliter [17], chitosan [18], carbon nanomaterials [19,20], activated carbon [21], etc. However, these adsorbents lack selectivity; as a result, the competitive adsorption of other common inorganic and/or organic compounds existing in water leads to low removal efficiency. Therefore, selective adsorbents are highly attractive in adsorption removal of BPA in water.

Molecularly imprinted polymers (MIPs) are synthetic receptors with specific binding sites. MIPs can selectively bind template molecules and its structure analogs. Because of the advantage, MIPs have been used widely for selective removal of target pollutants [22]. However, bulk MIPs prepared by traditional bulk polymerization have some shortcomings, including small capacity and poor binding kinetics, resulting in insufficient removal efficiency. Compared with bulk MIPs, molecularly imprinted nanoparticles (MINPs) have abundant binding sites for the binding of target compounds due to its large surface area and accessible sites. MINPs are usually prepared by direct precipitation polymerization or in-situ polymerization on the surface of various nanomaterials through surface molecular imprinting technology. Water compatibility should be considered for the application of MINPs in aqueous solutions. Some hydrophilic MINPs have been reported by using hydrophilic monomers during the preparation of MINPs or post-modifications of MINPs with hydrophilic molecules/polymer brushes [23-25]; however, the present hydrophilic monomers are related limited and the post-modifications are complicated. In addition, the separation of hydrophilic MINPs by filtration or centrifugation is difficult once they are completely dispersed in water, therefore cycle use of MINPs is difficult.

Dopamine (DA) is an import neurotransmitter, which easily suffers from a self-polymerization in weak alkaline condition to form

†To whom correspondence should be addressed.
E-mail: tanf@dlut.edu.cn

polydopamine (PDA). PDA has shown super adhesion ability on various material surfaces, good environmental stability, biocompatibility, and hydrophilicity [26]. Three-dimensional imprinted sites are achieved when a template is added during the self-polymerization, achieving specific recognition ability for the template. In addition, the thickness of PDA film can be precisely controlled by changing the polymerization time; therefore, it is convenient to obtain ultrathin imprinted PDA film on the surface of various nanomaterials. For example, several PDA-based imprinted nanomaterials, including IPDA@graphene [27], IPDA@multi-walled carbon nanotubes [28], and PDA nanowires [29], have been prepared for the separation of proteins in biological samples. PDA-based magnetic imprinted nanoparticles have been used for the enrichment and separation of glycopeptides and methylene blue in aqueous solutions [30,31].

In the present study, hydrophilic PDA-coated Fe_3O_4/graphene oxide (IPDA@MGO) magnetic imprinted nanocomposites were prepared by the self-polymerization of dopamine on the surface of Fe_3O_4/GO using BPA as a template in Tris-HCl buffer. The nanocomposites were characterized and its recognition abilities including adsorption capacity, binding kinetics and selectivity were evaluated. The effects of the template concentration and solution pH were also optimized. IPDA@MGO-based imprinting recognition coupled with magnetic separation resulted in fast removal of BPA in water. The present study proposes an efficient approach for adsorption removal of BPA in natural water.

EXPERIMENTAL

1. Materials

BPA, 4,4′-(hexafluoroisopropylidene)diphenol (BPAF), nonyl phenol (NP), bisphenol B (BPB), dopamine (DA), and tris(hydroxymethyl) aminomethane hydrochloride (Tris-HCl) were purchased from Aladdin Biochemical Corp. (Shanghai). Graphene oxide (GO) powder was obtained from Nanjing XFNANO Materials Tech Co., Ltd. (Nanjing, China). Deionized (DI) water was prepared by a Milli-Q® ultrapure water system (Bedford, MA USA).

2. Apparatus

Transmission electron microscopy (TEM) images were obtained by an FEI Tecnai G220. Infrared analysis was completed by a Shimadzu Prestige-21FTIR spectrometer. Elemental characterization was performed by an Elementar Vario EL III element analyzer. Magnetic properties of the nanocomposites were tested by a JDM-13 vibrating magnetometer at 25 °C. Brunauer-Emmett-Teller (BET) surface area was measured by a Quantachrome Autosorb S14 at −196 °C. The water-contact angle of the nanocomposites was measured by a KINO SL200KB contact angle meter.

3. Preparation of IPDA@MGO Nanocomposite

Fe_3O_4/GO was first prepared by a hydrothermal method with minor modifications [32]. Briefly, 40 mg of GO was dispersed in 40 g of ethylene glycol under ultrasonication for 2 h, and then 0.2 g of $FeCl_3 \cdot 6H_2O$, 1.8 g of sodium acetate and 0.8 g of PEG-4000 were added in the suspension under vigorous magnetic stirring at ambient temperature for 2 h. The suspension was kept in a 50 mL Teflon lined autoclave reactor at 200 °C for 10 h. The resulting Fe_3O_4/GO precipitate was collected, adequately washed with DI water, and dried under vacuum.

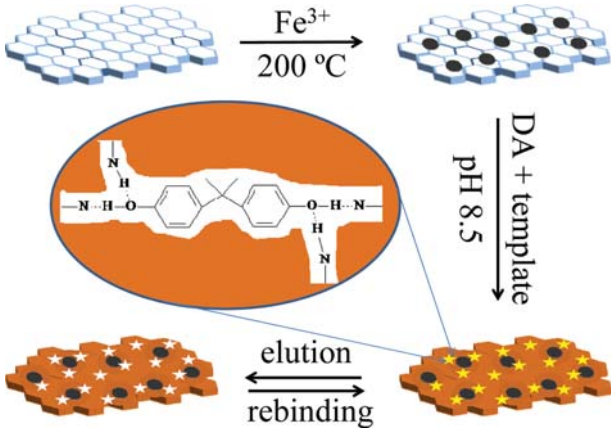

Scheme 1. A schematic diagram of IPDA@MGO preparation and its' selective recognition toward BPA.

The preparation of IPDA@MGO nanoparticles is shown in Scheme 1. 20 mg of Fe_3O_4/GO was dispersed in 25 mL ultrapure water under ultrasonication for 30 min and mixed with 15 mL of BPA-ethanol solution (0.5 mM), 5 mL of dopamine (5 g/L), and 5 mL Tris-HCl (0.2 M, pH 8.5). The suspension suffered a polymerization reaction at ambient temperature for 2 h. This process resulted in a PDA film on the surface of Fe_3O_4/GO. The resulting products were removed and adequately washed with a methanol/acetic acid (v/v=9 : 1) till BPA was not detected in the washing solution by HPLC, and dried under vacuum. The imprinted sites exposed once the removal of the embedded template in the PDA film. Nonimprinted PDA-coated Fe_3O_4/graphene oxide imprinted (NPDA@MGO) were prepared by the same procedures in the absence of BPA.

4. Sorption Experiments

Batch sorption experiments of BPA with the nanocomposites were carried out at ambient temperature. For the determination of adsorption capacity, 2 mg of IPDA@MGO and NPDA@MGO nanoparticles were added into 8 mL of BPA solution with concentrations ranging from 1 to 500 μM, respectively. After being shaken for 24 h, the nanocomposites were removed by a magnet, and 0.5 mL of the supernatant was collected and analyzed by HPLC. For binding kinetics study, 2 mg of the nanocomposites and 8 mL of BPA solution (400 μM) was mixed, and 20 μL of the supernatant was drawn at 1, 3, 5, 10, 30, 60, 90, and 120 min and analyzed by HPLC, respectively. All batch experiments were carried out in triplicate and the mean values were reported.

5. Selective Binding Experiments

To investigate the selectivity of IPDA@MGO, 2 mg of the nanocomposites were added into 8 mL of the mixed solution containing BPA, BPB, BPAF, and NP (the final concentration of BPA, BPB and BPAF is 10 μM, and the final concentration of NP is 50 μM). After being shaken at 25 °C for 120 min, the nanocomposites were removed by a magnet and the supernatant was removed for HPLC analysis. The adsorbed amount of BPA on the nanocomposites was calculated by the different value between the added amount and the remained amount in the supernatant. The same adsorption experiments were carried out for NPDA@MGO. Relative

imprinting factors (IF) between IPDA@MGO and NPDA@MGO toward BPA were calculated by the following equation.

$$IF=q_{MIP}/q_{NIP} \quad (1)$$

Where q_{MIP} and was q_{NIP} are the largest adsorption capacities of IPDA@MGO and NPDA@MGO to ward BPA at adsorption equilibrium, respectively.

6. Regeneration Experiments

To evaluate the reusability of IPDA@MGO, consecutive adsorption and desorption cycles was carried out with IPDA@MGO for 50 μM of BPA aqueous solution. After each adsorption, the nanocomposites were removed by a magnet and were eluted with 2 mL of methanol/acetonitrile (v/v=1 : 1) for three times, dried under vacuum, and reused for the adsorption of BPA in water.

7. Analytical Method

HPLC analysis was carried out by a Shimadzu Prominence LC-20A HPLC with a Shimadzu Shim-pack C18 (250 mm×4.6 mm, 5 μm) separation column and a UV detector at a detection wavelength of 220 nm. The mobile phase was water/acetonitrile (v/v= 40 : 60) with a flow rate of 1.0 mL/min. 20 μL of sample solution were injected for HPLC analysis.

RESULTS AND DISCUSSION

1. Characterization of Nanocomposites

The prepared nanocomposites were characterized by Fourier infrared spectra. There was an absorption peak at 580 cm^{-1} for Fe_3O_4/GO, IPDA@MGO, and NPDA@MGO, as shown in Fig. 1, which corresponds to the stretching vibration of Fe-O bond. The two peaks at 1,720 cm^{-1} and 1,580 cm^{-1} were attributed to the stretching vibrations of C=O and C=C of GO, respectively. The wide peak at approximate 3,410 cm^{-1} was attributed to the stretching vibration of -NH_2 group. Elemental analysis showed that the contents of nitrogen in IPDA@MGO and NPDA@MGO were 1.91% and 2.09%, respectively, while nitrogen was not found in Fe_3O_4/GO (Table 1). These results indicated that PDA was successfully formed on the surface of Fe_3O_4/GO through the self-polymerization of dopamine.

Fig. 2 shows the transmission electron microscopy (TEM) images of the prepared Fe_3O_4/GO and IPDA@MGO at different magnifications. Fe_3O_4 nanoparticles had mean diameters of 80-100 nm, which were tightly attached onto the surface of GO (Fig. 2(a). After

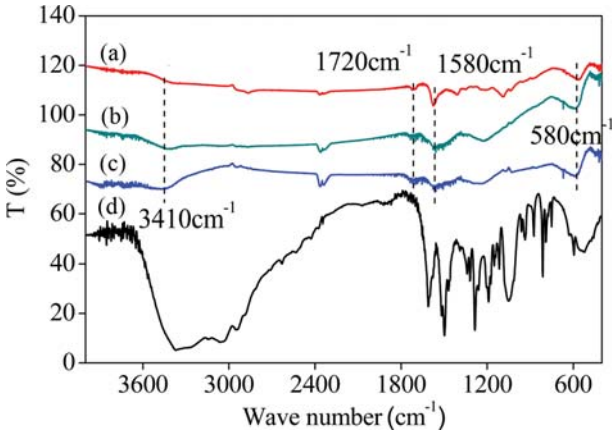

Fig. 1. FTIR spectra of Fe_3O_4/GO (a), NPDA@MGO (b), IPDA@MGO (c), and PDA nanocomposites (d).

Table 1. Elemental analysis of Fe_3O_4/G, IPDA@MGO, and NPDA@MGO

Elements	Elemental content (%)		
	IPDA@MGO	NPDA@MGO	Fe_3O_4/GO
N	1.91	2.09	0.00
C	29.11	22.85	21.06
H	1.42	1.37	1.816

the self-polymerization of dopamine, a thin IPDA film was clearly observed on the surface of Fe_3O_4/GO (Fig. 2(b) by the TEM image. The average thickness of the IPDA film was approximate 6-8 nm based on the scale bar in the TEM image. The thin IPDA film facilitated the template molecules into the inner imprinted sites, resulting in fast binding and adsorption equilibrium. NPDA@MGO had a similar NPDA film on the surface of Fe_3O_4/GO without no imprinted sites (Figure not shown).

Surface area is an important parameter for adsorbents. Generally, the adsorbents with large surface area have abundant binding sites and then large adsorption capacity. S_{BET} values of Fe_3O_4/GO, IPDA@MGO, and NPDA@MGO composites were measured by N_2 adsorption/desorption isotherms. Results showed that IPDA@MGO had the largest S_{BET} value (52.34 m^2/g), followed by Fe_3O_4/GO (40.33 m^2/g) and NPDA@MGO (46.32 m^2/g). The increased

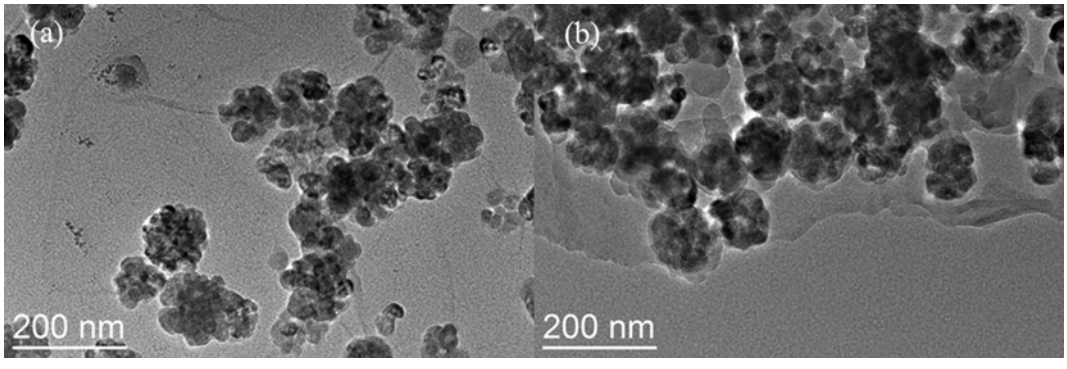

Fig. 2. TEM images of Fe_3O_4/GO (a) and IPDA@MGO (b) at different magnifications.

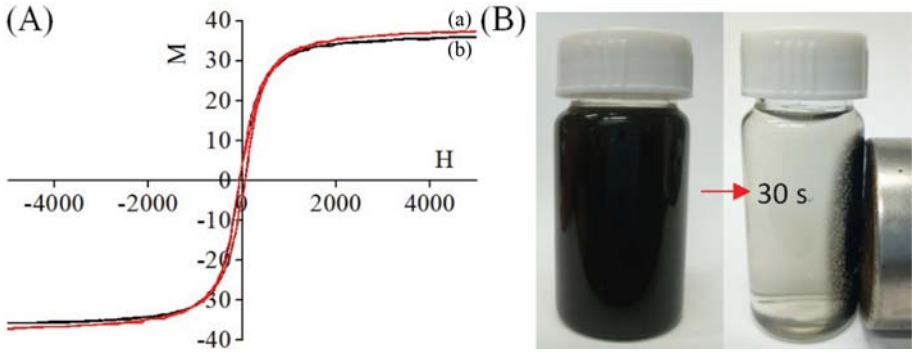

Fig. 3. Magnetization curves of Fe_3O_4/GO (a) and IPDA@MGO (b) (A) and separation of IPDA@MGO (B) by an external magnet.

S_{BET} value of IPDA@MGO compared with Fe_3O_4/GO and NPDA@MGO attributed to the contribution of the imprinted sites in the IPDA film.

To explore the feasibility of magnetic separation for the nanocomposites in water after each adsorption, the magnetization curves of Fe_3O_4/GO and IPDA@MGO were measured. As shown in Fig. 3(A), there were typical superparamagnetic properties. The saturation magnetizations were 37.1 and 35.6 emu/g for PDA@MGO and IPDA@MGO, respectively. The similar saturation magnetizations indicated that the introduction of IPDA film had no almost effect on the original magnetic property of Fe_3O_4/GO. The large saturation magnetization allowed for quick and complete isolation of IPDA@MGO in water by magnetic separation. Fig. 3(B) shows that the well dispersed IPDA@MGO nanocomposites in water were separated completely within 30 seconds by an external magnet forming a transparent supernatant solution.

Increasing surface's hydrophilicity is advantageous for the dispersion of adsorbents in water and for improving the interaction between the adsorbents and target compounds. Fig. 4(A) shows that the static water contact angle of IPDA@MGO was smaller than that of Fe_3O_4/GO (detailed data in Table 2). It was attributed to the strong hydrophilicity of the IPDA film on the surface of Fe_3O_4/GO. To observe the dispersion stability of Fe_3O_4/GO and IPDA@MGO in water, the nanocomposites were ultrasonicated for three minutes and then stored under static condition. As shown in Fig. 4(B), Fe_3O_4/GO showed complete sedimentation within 10 minutes, while IPDA@MGO keeps well dispersion within one hour although it finally suffered from sedimentation due to the larger density of IPDA@MGO compared with water. The good dispersion stability is attributed to the excellent surface hydrophilicity of IPDA@MGO.

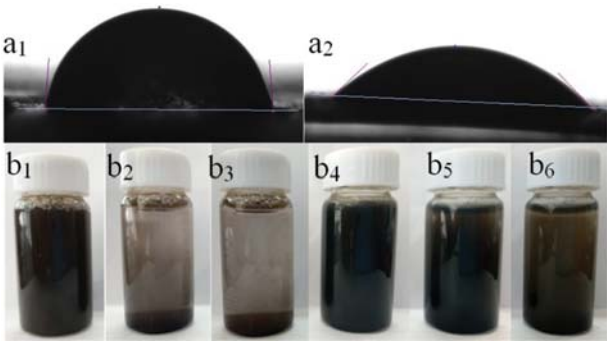

Fig. 4. (A) Static water contact angles of Fe_3O_4/GO (a1) and IPDA@MGO (a2). (B) photographs of Fe_3O_4/GO (b1-b3) and IPDA@MGO (b4-b6) suspension at 0 min (b1 and b4), 10 min (b2 and b5), and 60 min (b3 and b6) after ultrasonication for three minutes.

2. Optimization of Template Concentration

The recognition sites in MIPs highly depend on the amount of template used in the preparation, so the template concentration has an important effect on the adsorption performance of IPDA@MGO. Here IPDA@MGO nanocomposites were prepared by using three different template concentrations (40 μM, 150 μM and 500 μM). Fig. 5 shows the adsorption isotherms of BPA on the IPDA@MGO composites. All the adsorptions reached equilibriums when BPA concentrations increased to 80 mg/L. The largest

Table 2. Static water contact angles of Fe_3O_4/G (a1) and IPDA@MGO (a2) composites

	Volume of liquid drop (μL)	Left contact angle	Right contact angle	Average contact angle
Fe_3O_4/G	54.42	85.75	86.14	85.94
IPDA@MGO	42.09	36.88	36.35	36.61

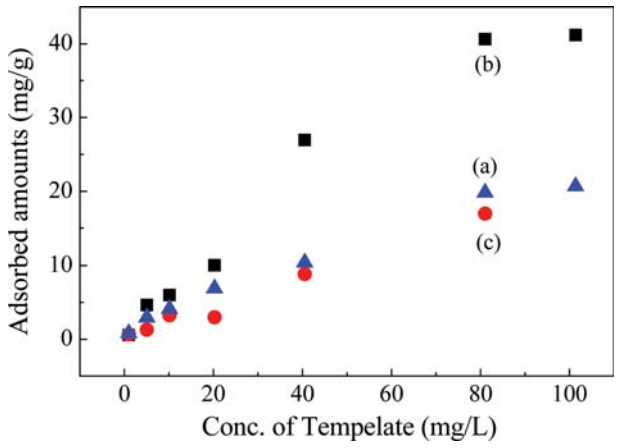

Fig. 5. Effect of the template concentration on the adsorbed amount of IPDA@Fe_3O_4/G toward BPA. 40 μM (a), 150 μM (b), and 500 μM (c).

adsorbed amount was obtained when 150 μM of template was used while 500 μM of template resulted in a low adsorbed amount (17.0 mg/g). This might be that excessive template restrained the self-polymerization of dopamine, resulting in the decrease of IPDA film thickness on Fe_3O_4/GO surface; as a result less binding sites were formed during the IPDA@MGO.

3. Adsorption Capacity of IPDA@MGO and NPDA@MGO Toward BPA

Fig. 6 shows the adsorption isotherms of BPA on IPDA@MGO and NPDA@MGO nanocomposites. The adsorbed amounts rapidly increased when BPA concentrations changed from 1 mg/L to 80 mg/L, while further increasing the concentration didn't result in obvious change of the adsorbed amount. This indicated that the adsorptions reached equilibriums. IPDA@MGO always achieved higher absorbed amounts compared with NPDA@MGO within the whole concentration range. The calculated maximum capacities based on the isotherms were 41.2 mg/g, and 11.5 mg/g for IPDA@MGO and NPDA@MGO, respectively. The binding of NPDA@MGO toward BPA was attributed to the nonspecific recognition by the hydrogen-bonding interaction between the hydroxyl groups of BPA and -NH_2 group of NPAD film. The binding ability was further enhanced when the imprinted sites were created for IPDA@MGO, resulting in a larger adsorption capacity. The relative IF calculated by the Eq. (1) was 3.58. The present IF was larger than those of previous studies [33-38], showing excellent recognition ability of the prepared IPDA@MGO toward BPA in water. Table 4 showed the adsorption capacities of IPDA@MGO and previous reported molecularly imprinted composites toward BPA.

Both Langmuir and Freundlich adsorption models are widely used to explain the adsorption mechanism of compounds on adsorbents. The present experimental data obtained by IPDA@MGO and NPDA@MGO were applied to the two adsorption models. Results showed that Freundlich equation gave larger r^2 values (>0.97) than those of Langmuir equation for the adsorption data (Table 3). This suggested that the adsorption followed Freundlich adsorption model. Fig. 6 shows that the experimental data matched well with the predication value by Freundlich model.

4. Binding Kinetics and Adsorption Equilibrium

The binding kinetic curves of IPDA@MGO and NPDA@MGO nanocomposites for BPA in water are shown in Fig. 7. The binding amounts of BPA on the nanocomposites rapidly increased with the incubation time within the initial 10 min and then had slow

Table 3. Fitting parameters of Langmuir and Freundlich equations for the adsorption of BPA on IPDA@MGO and NPDA@MGO nanocomposites

	Langmuir model		Freundlich model	
NPDA@MGO	b (mg/L)	31.72	n	0.5827
	q_m (mg/g)	15.01	k_F [mg/g(mL/mg)]	0.0015
	R^2	0.9433	R^2	0.9947
IPDA@MGO	b (mg/L)	195.85	n	0.9438
	q_m (mg/g)	129.87	k_F [mg/g(mL/mg)]	0.0013
	R^2	0.4971	R^2	0.9783

where q_e and q_m were the amount (mg/g) of BPA on the nanocomposites at equilibrium and the maximum capacity, respectively. C_e was the equilibrium concentration of BPA (mg/mL). b and K_F were the Langmuir and Freundlich constants, respectively, and n was the Freundlich exponent

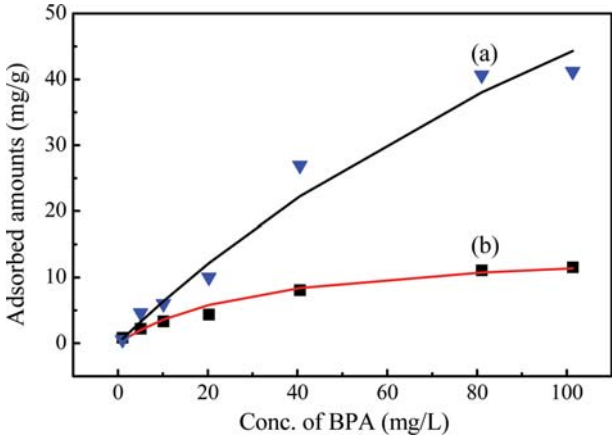

Fig. 6. Adsorption isotherms of IPDA@MGO (a) and NPDA@MGO (b) toward BPA. Symbols: experimental data; lines: Freundlich model predictions.

Table 4. Adsorption capacities of IPDA@MGO and previous reported molecularly imprinted composites toward BPA

MIP composites[a]	Monomer	Sorption capacity mg/g	Solution	Ref.
MIP@GO	AMPS and St	85.7	Water	[39]
MIP@FeOOH	MAA	36.9	Toluene/ACN	[40]
MIP@Fe_3O_4	4-VP	16.3	ACN	[41]
MIP@Fe_3O_4	MAA	3.9	Ethanol	[42]
MIP@β-cyclodextrin/chitosan /Fe_3O_4	MAA	105.5	Water	[43]
MIP@chitosan/γ-Fe_2O_3	MAA	135.1	Water	[44]
MIP@Fe_3O_4-COOH	APTES	91.7	Water	[45]
MIP@CMS	AMPS	5.4	Water	[46]
MIP@Styrene	VP and NIPAM	5.0	Water	[46]
MIP@SiO_2	DTPA	4.8-7.6	Water	[47]
IPDA@MGO	Dopamine	41.2	Water	This work

[a]ACN: acetonitrile; CMS: carbon microspheres; VP: 4-vinylpyridine; NIPAM: N-isopropylamide; VTES: vinyl-triethoxysilane

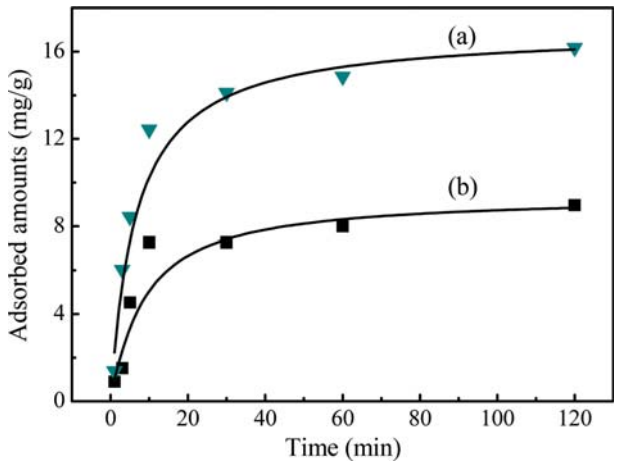

Fig. 7. Adsorption kinetic curves of IPDA@MGO (a) and NPDA@MGO (b) for BPA in water. Symbols: experimental data; lines: model predictions with the pseudo-second order kinetic model.

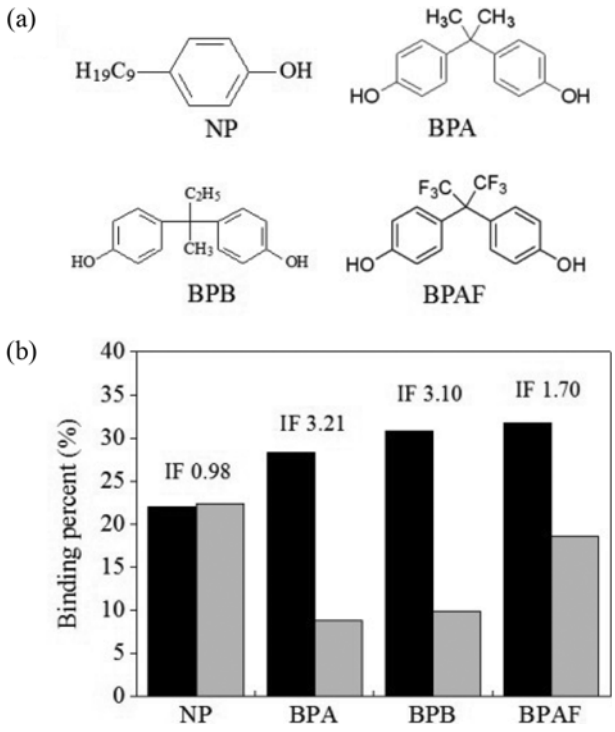

Fig. 8. (a) Molecular structures of NP, BPA, BPB, and BPAF, (b) binding percent of NP, BPA, BPB, and BPAF on IPDA@MGO (black) and NPDA@MGO (grey) in the mixed solution. Final concentration: 10 μM of BPA, BPB, and BPAF and 50 μM of NP.

increase with the time. The experimental data were applied to the pseudo first and second order models. Result showed that the pseudo second order model gave better correlation coefficients (r^2>0.999) than that of the pseudo first order model (Table 5), and the prediction results agreed well with the experimental data. This fact suggested that the adsorption of BPA on the nanocomposites was controlled by the chemisorption as a rate-limiting step. The initial adsorption rate on IPDA@MGO was three times more than that on NPDA@MGO (Table 5). The large sorption rates indicated that there were a lot of available binding sites. The adsorptions approached equilibriums at approximate 30 min. The short equilibrium time was attributed to the excellent binding characteristic of IPDA@MGO toward BPA and good dispersibility of the nanocomposites in water.

5. Effect of Solution pH

Solution pH has an effect on the surface charge density of adsorbents but also influences the speciation of target compounds in aqueous solutions. Previous studies showed that various MIPs had the largest adsorbed amount at pH 3.0 [48], 4.0 [33,38], or 5.0 [49]. Here the effect of solution pH in the range from 4.1 to 9.7 on the adsorption was studied. The largest adsorbed amount was obtained at ~pH 7.0, and the adsorbed amounts decreased rapidly in acidic and alkaline solutions. The adsorption could be explained by the π-π interaction between the phenyl groups of BPA and the phenyl rings of IPDA, and the hydrogen-bonding interaction between the hydroxyl groups of BPA and -NH_2 group of IPAD. At pH 7.0, BPA presented as neutral molecules while the surface of IPDA had little charges. This resulted in strong interactions and then large capacity. At acidic solution, abundant positive charges on the surface of IPDA reduced the interactions; at high pH, the repulsive force deriving from the negative charges of BPA and the surface of IPDA restrained the interactions, obtaining low adsorption capacity. It should be noted that the optimized pH in this study was different from that in previous MIPs, this was because that the present monomer (dopamine) had a larger pKa (8.9) than that of the previous monomers used in the reported MIPs, the optimized pH transferred toward alkaline direction.

6. Specific Binding of IPDA@MGO Toward BPA

The largest advantage of MIPs is the specific binding ability to template and its structure analogs. To evaluate the binding specificity of IPDA@MGO toward BPA, the nanocomposites were used

Table 5. Kinetic parameters of the pseudo-first-order and pseudo-second-order equations for the adsorption of BPA on IPDA@MGO and NPDA@MGO nanocomposites

Adsorbents	Pseudo-first-order			Pseudo-second-order			
	k_1	q_e (Cal.)	r^2	k_2	q_e (Cal.)	v_0	r^2
IPDA@MGO	0.0373	9.39	0.8195	0.0117	16.72	3.28	0.999
NPDA@MGO	0.0432	6.94	0.9776	0.0115	9.57	1.05	1.000

where q_e and q_t were the amount (mg/g) of BPA on the nanocomposites at equilibrium and t (min), respectively, k_1 (min^{-1}) and k_2 ($mg \cdot g^{-1} \cdot min^{-1}$) were the pseudo first and pseudo second order rate constants, respectively, and v_0 was the initial rate

for a mixed solution containing BPA, BPAF, BPB, and NP. The molecular structure of BPA, BPAF, BPB, and NP were shown in Fig. 8(a), where BPA, BPAF, and BPB contained bisphenol structures while NP was a phenol with a straight C_9 chain.

As shown in Fig. 8(b), IPDA@MGO showed similar binding percent toward BPA, BPB, and BPAF in the mixed solution while NP had a lower binding percent though its concentration was five times more than that of BPA, BPAF and BPB. This was because that BPA, BPB, and BPAF had same bisphenol structures while the molecular structure of NP was great different from that of BPA. On the other hand, NPDA@MGO showed obvious different binding characteristics toward the four compounds compared with IPDA@MGO. The largest binding percent was obtained for NP due to its higher concentration than the other compounds, followed by BPAF, and then BPA and BPAB. The relative high binding of BPAF was attributed to the strong hydrogen-bonding interaction between the hydroxyl groups of BPA and -NH_2 group of NPDA@MGO. The higher binding percent with IPDA@MGO toward BPA, BPB and BPAF containing bisphenol structures indicated that the imprinted sites played an important role for the competitive binding in the mixed solution. The relative IFs of the four compounds on IPDA@MGO and NPDA@MGO were 0.98 (NP), 3.21 (BPA), 3.10 (BPA), and 1.70 (BPAF) in the mixed solution by the Eq. (1), respectively. BPA gave the largest IF, while NP had no almost binding difference between IPDA@MGO and NPDA@MGO. This further confirmed the specific binding of that IPDA@MGO toward the template and its structure analogs rather than other compounds (Fig. 7(a)).

7. Repeated Adsorption of BPA in Water with IPDA@MGO

The feasibility of IPDA@MGO for removing BPA from water was evaluated with tap water spiked with BPA. After each adsorption, the nanocomposites were removed by an external magnet, washed with methanol/acetonitrile (v/v=1 : 1), and then reused for the adsorption of BPA in the water. Results showed that the sorption capacities of IPDA@MGO toward BPA were no any loss in five consecutive adsorption-regeneration cycles (41.18, 41.50, 38.44, 40.45, and 40.53 mg/g, with a RSD of 1.19%). This fact showed that the performance of IPDA@MGO was enough stable. Therefore, the prepared IPDA@MGO coupled with magnetic separation was feasible for efficient removal of BPA in water. The demonstrated reusability presents an advantage over some traditional adsorbents such as activated carbon.

CONCLUSION

Highly hydrophilic IPDA@MGO magnetic imprinted nanocomposites were prepared by the self-polymerization of dopamine on the surface of Fe_3O_4/GO for efficient removal of BPA in water through specific recognition and magnetic separation. The concentration of template had an important effect on the adsorption capacity of IPDA@MGO and the optimized concentration was 150 μM. The nanocomposites showed excellent sorption kinetics. This was attributed to the abundant binding sites and rapid binding of BPA in the imprinted sites. The largest adsorption capacity (41.2 mg/g) was at pH 7.0. The adsorption potential was mainly attributed to the π-π and hydrogen-bonding interactions between BPA and IPDA@MGO nanocomposites. The nanocomposites could be facilely separated by an external magnet following the adsorption and was regenerated by solvent washing for repeated uses in the removal of BPA in water without loss of removal efficiency. We believe that the nanocomposites have potential applications in efficient removal of BPA in environmental waters.

ACKNOWLEDGEMENT

The work was supported by the National Natural Science Foundation of China (No. 21577010), the Dalian Municipal Fund for High-level (Leading) Professionals (2015R011), the Fundamental Research Funds for the Central Universities (DUT18LAB14), and the Programme of Introducing Talents of Discipline to Universities (B13012).

COMPETING FINANCIAL INTERESTS

The author(s) declare no competing financial interests

REFERENCES

1. P. Macikova, K. J. Groh, A. A. Ammann, K. Schirmer and M. J. F. Suter, *Environ. Sci. Technol.*, **48**, 12902 (2014).
2. V. S. Wilson, M. C. Cardon, L. E. Gray, Jr. and P. C. Hartig, *Environ. Toxicol. Chem.*, **26**, 1793 (2007).
3. F. Tan, H. X. Zhao, X. N. Li, X. Quan, J. W. Chen, X. M. Xiang and X. Zhang, *J. Chromatogr. A*, **1216**, 5647 (2009).
4. I. A. Lang, T. S. Galloway, A. Scarlett, W. E. Henley, M. Depledge, R. B. Wallace and D. Melzer, *JAMA-J. Am. Med. Assoc.*, **300**, 1303 (2008).
5. N. Salgueiro-Gonzalez, E. Concha-Grana, I. Turnes-Carou, S. Muniategui-Lorenzo, P. Lopez-Mahia and D. Prada-Rodriguez, *J. Chromatogr. A*, **1223**, 1 (2012).
6. G. M. Klecka, C. A. Staples, K. E. Clark, N. van der Hoeven, D. E. Thomas and S. G. Hentges, *Environ. Sci. Technol.*, **43**, 6145 (2009).
7. V. A. Santhi, N. Sakai, E. D. Ahmad and A. M. Mustafa, *Sci. Total Environ.*, **427**, 332 (2012).
8. Z. Fan, J. Hu, W. An and M. Yang, *Environ. Sci. Technol.*, **47**, 10841 (2013).
9. E. J. Rosenfeldt and K. G. Linden, *Environ. Sci. Technol.*, **38**, 5476 (2004).
10. B. Seyhi, P. Drogui, G. Buelna, A. Azais and M. Heran, *Environ. Pollut.*, **180**, 229 (2013).
11. C. Huang, P. Xu, G. Zeng, D. Huang, C. Lai, M. Cheng, L. Deng, C. Zhang, J. Wan and L. Liu, *Appl. Microbiol. Biotechnol.*, **101**, 3919 (2017).
12. M. Gmurek, M. Olak-Kucharczyk and S. Ledakowicz, *Chem. Eng. J.*, **310**, 437 (2017).
13. Y. Zhang, C. Causserand, P. Aimar and J. P. Cravedi, *Water Res.*, **40**, 3793 (2006).
14. A. Bhatnagar and L. Anastopoulos, *Chemosphere*, **168**, 885 (2017).
15. M. R. Gandhi, S. Vasudevan, A. Shibayama and M. Yamada, *Chemistryselect*, **1**, 4358 (2016).
16. S. Zheng, Z. Sun, Y. Park, G. A. Ayoko and R. L. Frost, *Chem. Eng. J.*, **234**, 416 (2013).
17. N. Genc, O. Kilicoglu and A. O. Narci, *Environ. Technol.*, **38**, 424

(2017).
18. Y. Kimura, M. Yamamoto, R. Shimazaki, A. Kashiwada, K. Matsuda and K. Yamada, *J. Appl. Polym. Sci.*, **124**, 796 (2012).
19. J. Bohdziewicz and G. Kaminska, *Water Sci. Technol.*, **68**, 1306 (2013).
20. Z. Jin, X. Wang, Y. Sun, Y. Ai and X. Wang, *Environ. Sci. Technol.*, **49**, 9168 (2015).
21. Z. Gong, S. Li, J. Ma and X. Zhang, *Sep. Purif. Technol.*, **157**, 131 (2016).
22. Z. H. Meng, W. Chen and A. Mulchandani, *Environ. Sci. Technol.*, **39**, 8958 (2005).
23. Y. Ma, G. Pan, Y. Zhang, X. Guo and H. Zhang, *Angew. Chem. Int. Ed.*, **52**, 1511 (2013).
24. J. Matsui, K. Tamaki and N. Sugimoto, *Anal. Chim. Acta*, **466**, 11 (2002).
25. J. Haginaka and H. Sanbe, *Anal. Chem.*, **72**, 5206 (2000).
26. H. Lee, S. M. Dellatore, W. M. Miller and P. B. Messersmith, *Science*, **318**, 426 (2007).
27. J. Luo, S. Jiang and X. Liu, *J. Phys. Chem. C*, **117**, 18448 (2013).
28. R. Liu, M. Sha, S. Jiang, J. Luo and X. Liu, *Talanta*, **120**, 76 (2014).
29. R. Z. Ouyang, J. P. Lei and H. X. Ju, *Chem. Commun.*, 5761 (2008).
30. F. Meng, W. Wei, J. Chen, X. Chen, X. Xu, M. Jiang, Y. Wang, J. Lu and Z. Zhou, *RSC Adv.*, **5**, 101121 (2015).
31. C. Bi, R. Jiang, X. He, L. Chen and Y. Zhang, *RSC Adv.*, **5**, 59408 (2015).
32. F. Tan, M. Liu and S. Y. Ren, *Sci. Rep.*, **7**, 1 (2017).
33. G. Bayramoglu, M. Y. Arica, G. Liman, O. Celikbicak and B. Salih, *Chemosphere*, **150**, 275 (2016).
34. F. Duan, C. Chen, X. Zhao, Y. Yang, X. Liu and Y. Qin, *Environ. Sci. Nano.*, **3**, 213 (2016).
35. X.-B. Zhang, J. Li, B. You, G.-P. Yong, H.-W. Tong and S.-M. Liu, *RSC Adv.*, **2**, 9778 (2012).
36. Y. Zhang, Q. Wei, Q. Zhang, J. Li, J. Yang and C. Zhao, *Sep. Sci. Technol.*, **46**, 1615 (2011).
37. T. Chang, Y. Liu, X. Yan, S. Liu and H. Zheng, *RSC Adv.*, **6**, 66297 (2016).
38. F. Duan, C. Chen, L. Chen, Y. Sun, Y. Wang, Y. Yang, X. Liu and Y. Qin, *Ind. Eng. Chem. Res.*, **53**, 14291 (2014).
39. F. F. Duan, C. Q. Chen, X. F. Zhao, Y. Z. Yang, X. G. Liu and Y. Qin, *Environ. Sci. Nano*, **3**, 213 (2016).
40. S. M. Amininasab, P. Holakooei, Z. Shami and M. Hassanzadeh, *J. Polym. Res.*, **25**, 1 (2018).
41. J. Liu, W. Wang, Y. Xie, Y. Huang, Y. Liu, X. Liu, R. Zhao, G. Liu and Y. Chen, *J. Mater. Chem.*, **21**, 9232 (2011).
42. N. Griffete, H. Li, A. Lamouri, C. Redeuilh, K. Chen, C. Z. Dong, S. Nowak, S. Ammar and C. Mangeney, *J. Mater. Chem.*, **22,** 1807 (2012).
43. D. L. Huang, Z. H. Tang, Z. W. Peng, C. Lai, G. M. Zeng, C. Zhang, P. A. Xu, M. Cheng, J. Wan and R. Z. Wang, *J. Taiwan Inst. Chem. Eng.*, **77**, 113 (2017).
44. J. M. Pan, W. Hu, X. H. Dai, W. Guan, X. H. Zou, X. Wang, P. W. Huo and Y. S. Yan, *J. Mater. Chem.*, **21**, 15741 (2011).
45. T. T. Chang, Y. X. Liu, X. Y. Yan, S. M. Liu and H. S. Zheng, *RSC Adv.*, **6**, 66297 (2016).
46. F. F. Duan, C. Q. Chen, L. Chen, Y. J. Sun, Y. W. Wang, Y. Z. Yang, X. G. Liu and Y. Qin, *Ind. Eng. Chem. Res.*, **53**, 14291 (2014).
47. Y. M. Ren, J. Yang, W. Q. Ma, J. Ma, J. Feng and X. L. Liu, *Water Res.*, **50**, 90 (2014).
48. W. Guo, W. Hu, J. Pan, H. Zhou, W. Guan, X. Wang, J. Dai and L. Xu, *Chem. Eng. J.*, **171**, 603 (2011).
49. M. H. Dehghani, M. Ghadermazi, A. Bhatnagar, P. Sadighara, G. Jahed-Khaniki, B. Heibati and G. McKay, *J. Environ. Chem. Eng.*, **4**, 2647 (2016).